EXPERIMENTAL INVESTIGATION OF A FLOW AROUND A SPHERE

by

Vukman BAKIĆ

This paper presents the experimental results for the flow around a sphere: a smooth sphere in flow with low inlet turbulence, a sphere with trip wire, and a sphere in flow with high free stream turbulence, at subcritical Reynolds number. The mean velocity field and the turbulence quantities are obtained using laser-Doppler anemometry. Comparison of velocity field and turbulence characteristics for different flow configuration are given.

Key words: *sphere, turbulence, laser-Doppler anemometry, grid, trip wire*

Introduction

Many bodies of practical interest are bluff, and there are lots of studies which deal with various aspects of the complex flow around them. The sphere has been chosen as a representative example of bluff body without sharp edges which fix the flow separation, thus backing to flows similar to those found around many vehicle types. The main characteristic of such flows is the existence of turbulent wake with recirculation, which has a dominant effect on the drag and lift of the body. The extent of this region is dependent on the shape, orientation and size of the body, the velocity and viscosity of the fluid, and may be influenced by a wide variety of small flow disturbances, which may be generated in various ways.

Flow around a sphere has been studied experimentally in numerous works. Most of the studies provided flow visualization, distribution of the wall skin friction coefficient and pressure around sphere, as well as integral parameters such as the drag coefficient or the wake frequencies of the shedding motion which occurs behind the sphere [1, 5, 7, 9]. Different flow regimes were determined experimentally: (1) the flow is laminar, and separation does not occur when the Reynolds number is lower than about 20; (2) separation occurs at Re 24 and results in the generation of a an axis symmetric rings which is stable for Reynolds number up to Re = 210 when the wake becomes non axis symmetric; (3) at Re = 270 wake becomes unstable, and vortex loops began to shed from the sphere; (4) when the Reynolds number is further increased to around 800, the vortex

loops diffuse very rapidly, and the wake flow becomes turbulent. The turbulent range can be subdivided into four regimes: (a) subcritical regime up to Re 330,000 where there is a laminar boundary layer separation occurs at about $\alpha_s = 81^o$ and position of separation remains almost unaltered over the range 10^4 Re $3.0 \cdot 10^5$ followed by transition to fully turbulent flow downstream 8, 12 ; (b) critical regime for Reynolds between 300,000 and 330,000 which is characterized by a significant drop of the drag coefficient; (c) supercritical regime between Re $3.3 \cdot 10^5$ to Re $2 \cdot 10^7$, and (d) transcritical regime for higher Reynolds numbers. Detailed experimental data on the mean flow structure and the structure of the turbulence are rare. Work [6] provides quantitative experimental data on the mean velocity and the Reynolds stresses. They used laser-Doppler anemometry (LDA) and investigated the flows around sphere at sub critical Reynolds number $5 \cdot 10^4$.

The use of surface roughness to trigger transition of the boundary layer is a common feature of many experiments. The technique is used for not only airfoil surfaces but for all types of body shapes and for applications wider than just in aeronautics. First well-known experiments with sphere and trip-wire have been done Wiselberger (1914) [13]. He analyzed the drag coefficient and visualized the flow over a sphere with trip-wire. Fage (1929) [3] analyzed the effects of turbulence and surface roughness on the drag of a circular cylinder. He showed that with increasing diameter of the trip-wire, the critical Reynolds number and drag coefficient decreased.

Most of experimentally studied flows around bluff bodies are performed in wind tunnels and in flows with low levels of free stream turbulence. However, in many practical situations bluff bodies are in the wake of another body or more general in a high turbulence level. Therefore, in this study measurements of the flow around a smooth sphere with a higher level of free-stream turbulence have also been performed.

In this paper experimental results of mean velocities and turbulence characteristics for a smooth sphere, a sphere with trip wire and a sphere in a flow with high free stream turbulence are given. The results are obtained using LDA.

Experimental setup

The experiment was conducted in a closed circuit type low speed wind tunnel. This tunnel has a contraction ratio of 1:4 and a test section with a square cross section 300 mm wide, 300 mm high and 600 mm long, with three turbulence suppressing screens upstream of the contraction. The tunnel operated with a wind speed of $U_0 = 12.6$ m/s. At this speed the free stream turbulence level, measured with hot-wire anemometry, was $(\overline{u^2})^{1/2}/U_0$ 0.0056. A sphere with diameter $D = 61.4$ mm was supported from the rear by a sting which had a length $5.7D$ and a diameter $d = 0.13D$. The blockage ratio was 3.2%. The Reynolds number based on sphere diameter and velocity of air U_0 was Re = 51,500.

A sphere with same diameter with trip-wire was used. The position of the trip wire with a diameter $d_t = 0.5$ mm is 75° from the front stagnation point. Separation of laminar boundary layer for a smooth sphere happed at 82° degrees from the stagnation point. This is reason why the position of trip wire must be at angle smaller than 82°.

The majority of investigations into effects of free-stream turbulence on flow around bluff bodies has been conducted in wind tunnels using grid/generated turbulence. The same approach has been adopted here. The grid was mounted at the entrance to the working section. The free/stream, turbulence decays downstream of the grid according to the following law, (Bradshow, 2002, private communication):

$$\frac{\sqrt{\overline{u^2}}}{U} \quad 10 \quad \frac{x}{M} \quad 4 \qquad (1)$$

where $(\overline{u^2})^{1/2}/U$ is turbulence intensity, x is distance from the grid and M is the mesh width (distance between bar centerlines). This law is valid for $M/b = 6.1$ where b is bar width and for $x/M > 10$. In this experiment $M = 30$ mm and $b = 5$ mm . The sphere with same diameter $D = 61.4$ mm was mounted $10\,M$ downstream of the grid. Measurements with LDA showed that turbulence intensity in this case at the sphere position was about 7.8%. The velocity was $U_0 = 11.1$ m/s. According to the mean velocity and sphere diameter the Reynolds number was about 48,000.

Velocity measurements have been carried out using two component forward laser-Doppler system manufactured by Technical Scientific Instruments (TSI). The 514.5 and 488 nm laser beams of an argon-ion laser were used to measure axial and radial components of velocity respectively. The optics to focus the laser beams consist of a fiber measuring probe and transmitting lens with a focal length of $f = 350$ mm. The distance between the laser beams at the transmitting lens was 50 mm. With this optical arrangement the dimension of the measuring volume was $0.091 \times 0.091 \times 1.279$ mm.

In the present experiments the air was seeded with water drops of the size of about 0.6-3 µm. They were injected in the tunnel at the end of test section. A small amount of glycerol added to the water prevented the water from evaporating and helped the drops to maintain their size. Frequency analysis of the governing equation of motion of the water drops illustrated that the drops could faithfully follow sinusoidal motions with frequencies up to 10 kHz. The selected maximum frequencies are typical for the maximum energy – containing frequencies in turbulent air flows.

Since the reversed flows needed to be measured, a frequency shift of 5 MHz was used on the green and 1 MHz for the blue systems which was based on the velocity range of interest. The signals were processed using a TSI, model IFA-750, signal processor in coincidence mode. Coincidence windows between 20-100 µs were used to get the Reynolds stress. Data acquisition and analysis is performed on a personal computer with the commercial TSI FIND software. For each position 20,480 data points are collected.

Results

Flow around a smooth sphere in flow with low inlet turbulence

The general character of sub-critical flow over a sphere is well understood. A laminar boundary layer forms on the upstream surface of the sphere. The flow accelerates as it is deflected by the sphere causing a sharp drop in pressure in stream-wise direction. For a Reynolds number of 51,500, the separation of laminar boundary layer hap-

pens at an angle between 80° and 83°. Behind the sphere a recirculation zone is formed, whose length is about $x/D = 1.43$ from the center of the sphere. The recirculation zone can be seen in fig. 1. Figure 2 shows contours of the axial velocity component U/U_0. The averaged axial velocity component has maximum values $U_{max} = 1.19\ U_0$ at the top of the sphere and the maximum reverse velocity is $U_{min} = -0.427\ U_0$. Figure 3 shows contours of radial velocity component V/U_0. The V component is positive in the region around the sphere and up to $x/D = 0.8$ with maximum values of $V/U_0 = 0.21$. The minimum value $V/U_0 = -0.11$ is found near re-attachment point at the position $x/D = 1.4$.
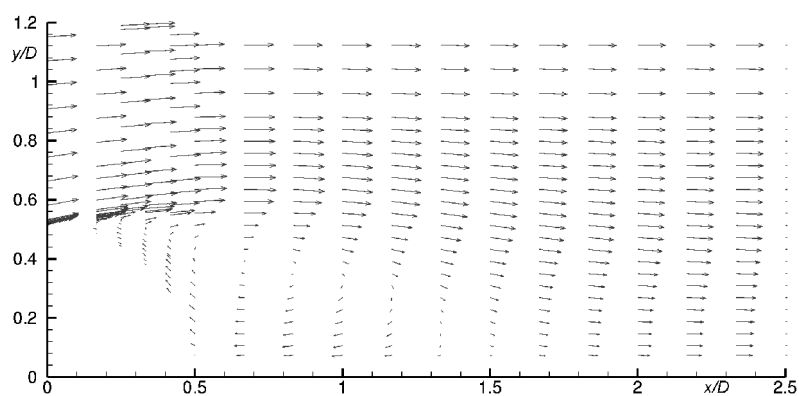
Figure 1. Measured mean velocity vectors behind sphere
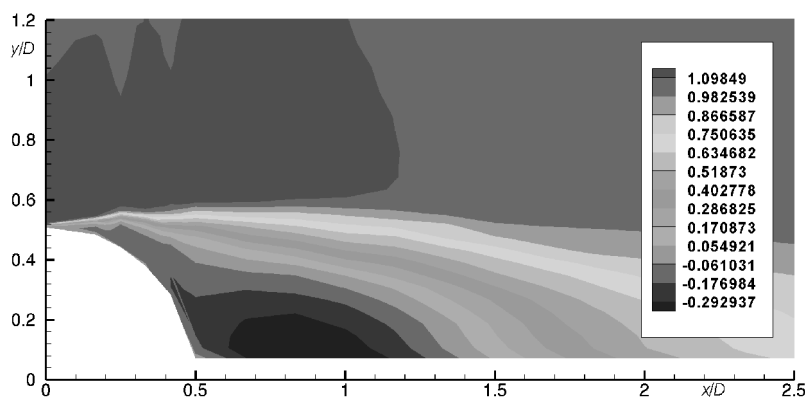
Figure 2. Contours of the measured axial velocity component U/U_0

Figures 4 and 5 show the turbulence intensity in the axial and radial directions $(\overline{u^2})^{1/2}/U_0$ and $(\overline{v^2})^{1/2}/U_0$ respectively, while fig. 6 shows the Reynolds stress $\overline{uv}/U_0^2$ The
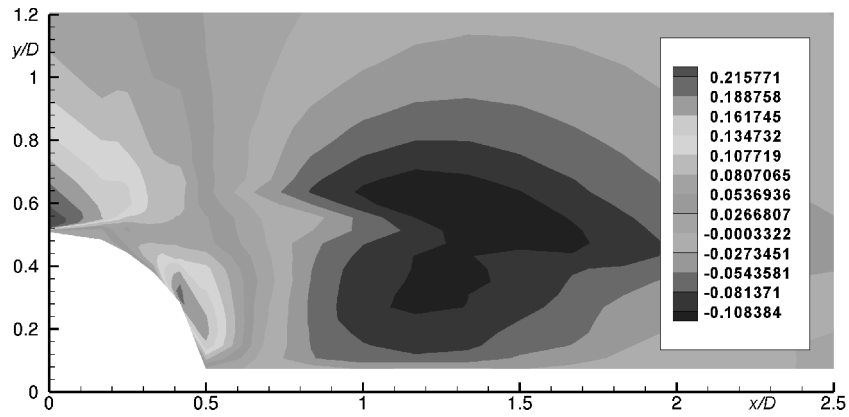
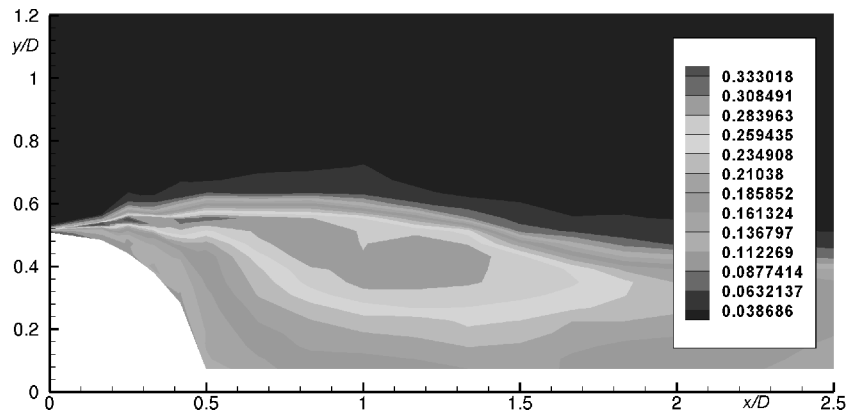**Figure 3. Contours of the measured radial velocity component V/U_0**

Figure 4. Contours of the measured turbulence intensity in axial direction $(\overline{u^2})^{1/2}/U_0$

turbulence intensity in axial direction $(\overline{u^2})^{1/2}/U_0$ is the largest with maximum values in the shear layer. Experimental investigation done in 5 showed that the maximum of axial turbulence intensity $(\overline{u^2})^{1/2}/U_0$ is found behind the sphere ($x/D > 0.5$), but this measurements and the large eddy simulation simulation done by Schmid [11] show that maximum of this turbulence intensity lies actually almost at the beginning of the free shear layer development. The width of the shear layer after separation is small and increase due to roll-up off the eddies. Direct numerical simulation of the flow around the sphere at Re = 5,000 [9] showed (with the help of invariant map) that the state of turbulence in the shear layer shortly after separation is nearly one-dimensional, with fluctuations primarily in stream-wise direction. After roll-up and brake-down of vortex ring, the turbulence becomes three-dimensional and attains a nearly isotropic state in the re-attachment zone.
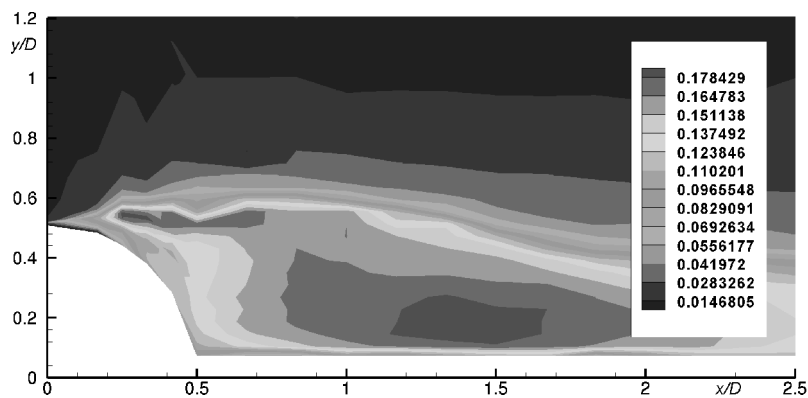
Figure 5. Contours of the measured turbulence intensity in radial direction $(\overline{v^2})^{\frac{1}{2}}/U_0$
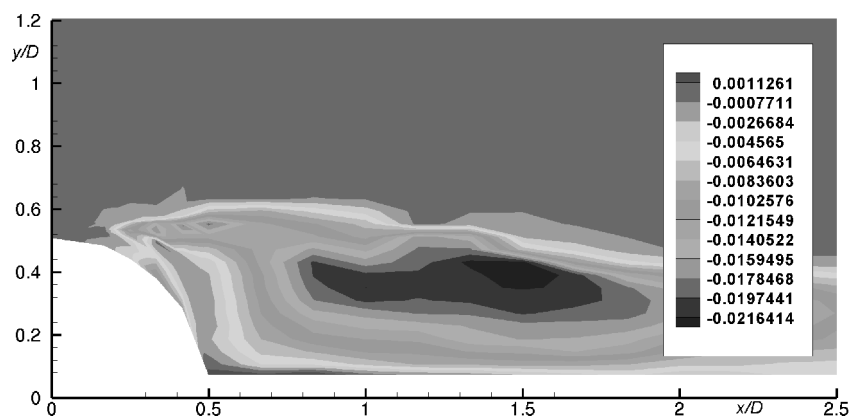

Figure 6. Contours of the measured Reynolds stress $\overline{uv}/U_0^2$

The value of the turbulence intensity in radial direction $(\overline{v^2})^{\frac{1}{2}}/U_0$ increased slowly in the shear layer and overtook the maximum at the end of the recirculation zone. The Reynolds stress $\overline{uv}/U_0^2$ is positive before transition and than becomes negative in the wake of the sphere.

Flow around a sphere with trip-wire

In most practical applications a trip-wire or other artificial roughness is used to promote transition of the boundary layer in order to achieve better similarity between model measurements and full-scale geometry.

68

Figure 8 shows the velocity vectors of the flow behind the sphere with trip-wire. From this and fig. 9 , which presents contours of the axial velocity U/U_0 it can be seen that the separation of boundary layer occurs at an angle about $\alpha_s = 120°$ from the front stagnation point. This can also be seen in fig. 7, which shows visualization of boundary layer separation by injection of dye, for the sphere with trip/wire. Visualization was done in water tank. The sphere and trip-wire had same dimensions as sphere and trip-wire in tunnel. Due to the delayed separation of the boundary layer at $\alpha_s = 120°$, the length of the separation zone, $L = = 1D$, is significantly shorter than in the case of the smooth sphere ($L = 1.43D$).

Figure 7. Visualization of boundary layer separation using dye in a water tank for the sphere with trip-wire

From this picture one can also see that the width of the wake and the shear layer are smaller than for the sphere without trip-wire. The trip-wire leads to an increase in velocity at the top of the sphere, see fig. 9. The maximal axial velocity is about $U/U_0 = 1.37$, while in the case of a smooth sphere, a maximum value of 1.19 was found. The maximal negative velocity in the recirculation zone is $U/U_0 = -0.24$, which is significantly less than in the case of a sphere without trip-wire, where negative values of the axial velocity around $U/U_0 = -0.45$ were measured. The radial velocity component has negative values immediately behind the top of the sphere, fig. 10, contrary to the pattern seen for the sphere without trip-wire, see fig. 3. This indicates that the flow follows the wall contour, while in the case of a smooth sphere it was still directed away from the symmetry axis.

Figures 11 and 12 show turbulence intensity in axial and radial directions $(\overline{u^2})^{1/2}/U_0$ and $(\overline{v^2})^{1/2}/U_0$, and fig. 13 shows Reynolds stress $\overline{uv}/U_0^2$. The turbulence in-
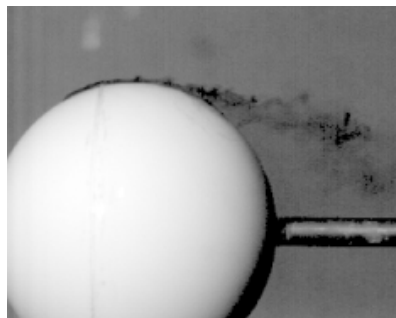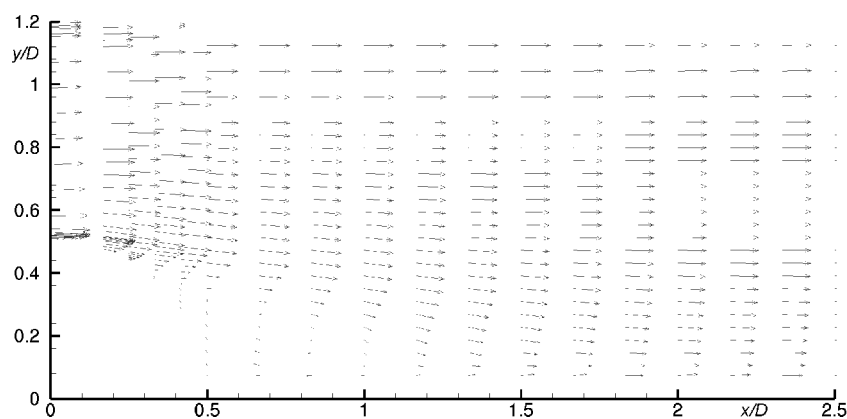

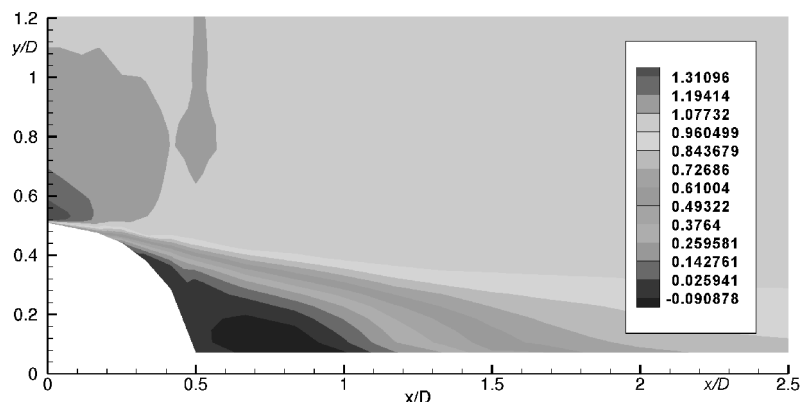**Figure 8. Measured mean velocity vectors behind sphere with trip-wire**

Figure 9. Contours of the measured axial velocity component U/U_0 for the sphere with trip-wire
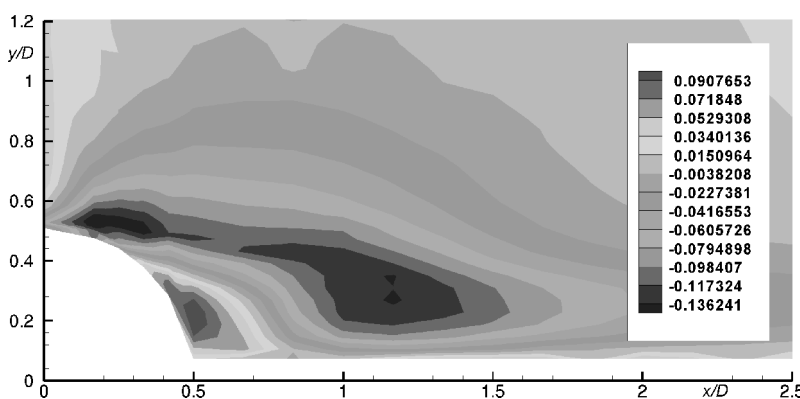

Figure 10. Contours of the measured radial velocity component V/U_0 for the sphere with trip-wire

tensities $(\overline{u^2})^{1/2}/U_0$ and $(\overline{v^2})^{1/2}/U_0$ have maximal values at the top of the sphere, with another maximum just behind the recirculation zone; as in the case of the smooth sphere, $(\overline{u^2})^{1/2}/U_0$ is largest at a about $x/D = 1.1$ and $y/D = 0.25$, while $(\overline{v^2})^{1/2}/U_0$ largest near the wall of supporting sting. Maximum values of Reynolds stress $\overline{uv}/U_0^2$ are found in the shear layer at the edge of the recirculation zone.

Flow around a sphere in a flow with high free–stream turbulence

The flow downstream of a grid does not have a uniform mean velocity profile due to the presence of the wakes behind the bars, but this non-uniformity decays very rapidly, much faster than the turbulence intensity. At a moderate distance downstream of the grid (10*M*), the non-uniformity of the velocity field is negligible. Figure 14 shows
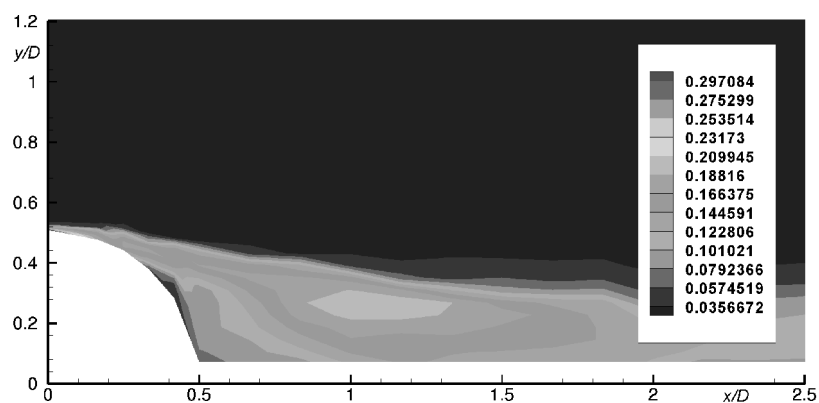
70

Figure 11. Contours of the measured axial turbulence intensity $(\overline{u^2})^{1/2}/U_0$ **for the sphere with trip-wire**
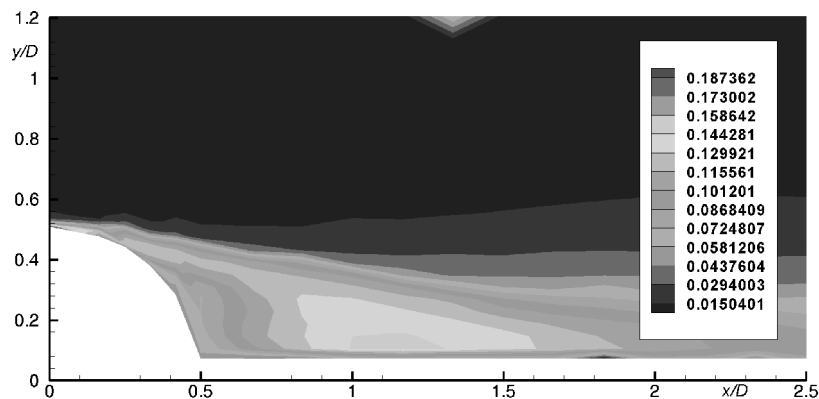

Figure 12. Contours of the measured radial turbulence intensity $(\overline{v^2})^{1/2}/U_0$ **for the sphere with trip-wire**
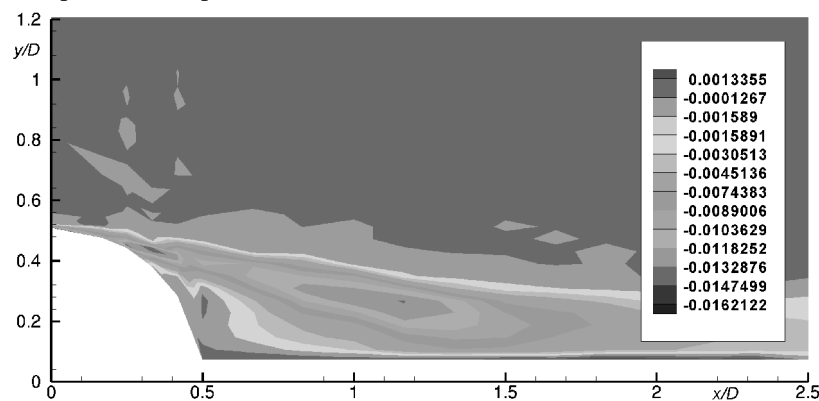

Figure 13. Contours of the measured Reynolds stress $\overline{uv}/U_0^2$ **for the sphere with trip-wire**
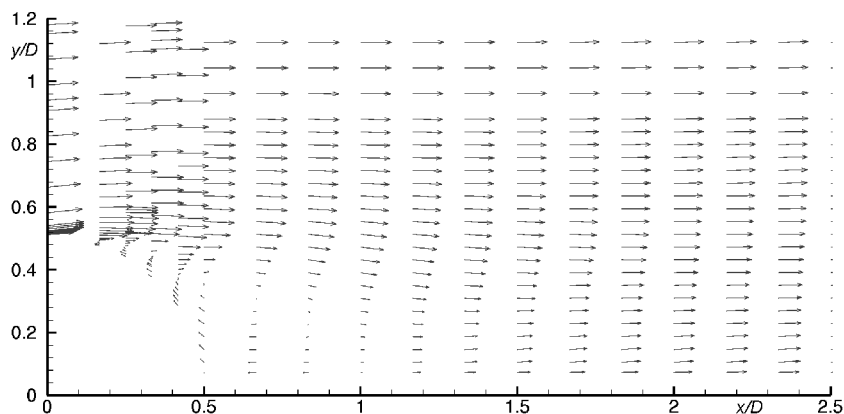
71

Figure 14. Measured mean velocity vectors behind sphere in a flow with high free-stream turbulence

the mean velocity vectors of flow behind the sphere in the case of high free stream turbulence. From this and the next fig. 15, which presents the contours of the mean axial velocity U/U_0, one can see that the separation point of the boundary layer is at about $\alpha_s = 101°$. Experimental investigation [12], for a smooth sphere in a low-turbulence flow, using oil coating visualization techniques showed that the boundary layer separates at $\alpha_s = 80°$ for Re $= 2.3 \cdot 10^4$, and that the position of separation remains almost unaltered over the range $10^4 <$ Re $< 3.5 \cdot 10^5$. Raithby and Eckert (1968) [8] used the same visualization techniques. They investigated the effect of support position and turbulence intensity on the flow near the surface of a sphere. Their results showed that with increasing free-stream turbulence, the position of separation point moves further downstream. This is the main reason why in this experiment, separation point is at about $\alpha_s = 101°$. Increas-
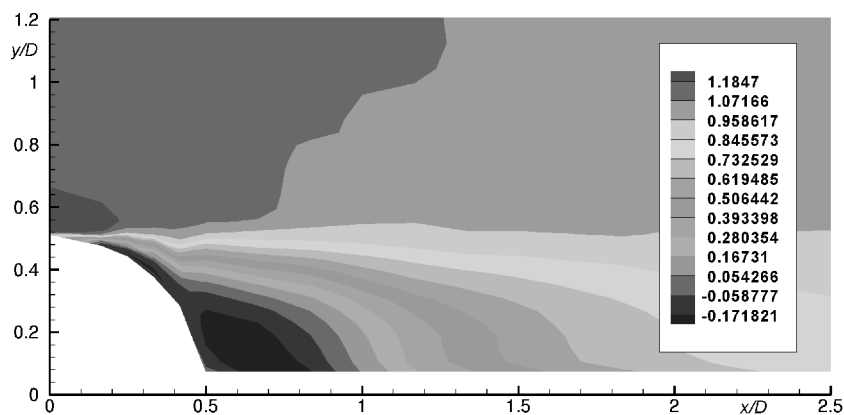

Figure 15. Contours of the measured axial velocity component U/U_0 behind sphere in a flow with high free-stream turbulence

72

ing the free stream turbulence leads to an increase in mixing and entrainment in the separated shear layer. Increasing the turbulence level in the free stream leads to an earlier transition to turbulence in the separated boundary layer. The entrainment increase always leads to the separated shear layer to bend towards the body. This is the reason why the length of the recirculation zone behind sphere in the flow with high free-stream turbulence is shorter ($L/D = 0.98$) than in the flow with low free-stream turbulence ($L/D = 1.43$). Berman's [2] measurement of the distance to re-attachment to along splitter plate in the wake of a square section cylinder shows also that the length of recirculation zone decreases with increasing the turbulence intensity in the free-stream. The maximal axial velocity is about $U/U_0 = 1.28$ at the top of the sphere and the minimal axial velocity is $U/U_0 = -0.28$ for $x/D = 0.667$. Figure 15 shows the contours of the mean radial velocity V/U_0. The maximal positive radial velocity is about $V/U_0 = 0.18$ close to sphere wall at $x/D = 0.333$. The maximal negative redial velocity is about $V/U_0 = -0.14$ at $x/D = 1.167$.
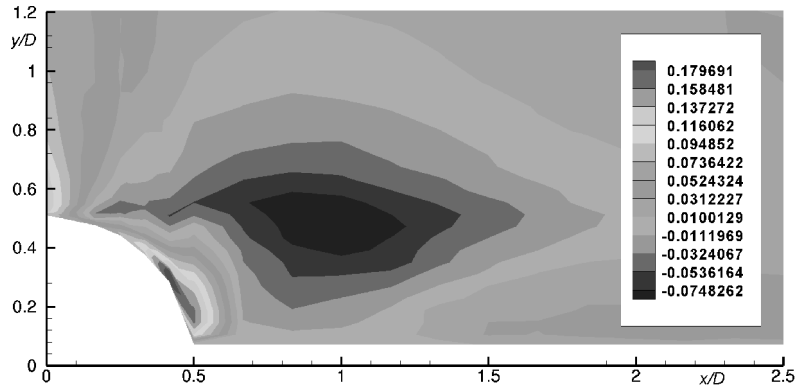

Figure 16. Contours of the measured radial velocity component V/U_0 behind sphere in a flow with high free-stream turbulence
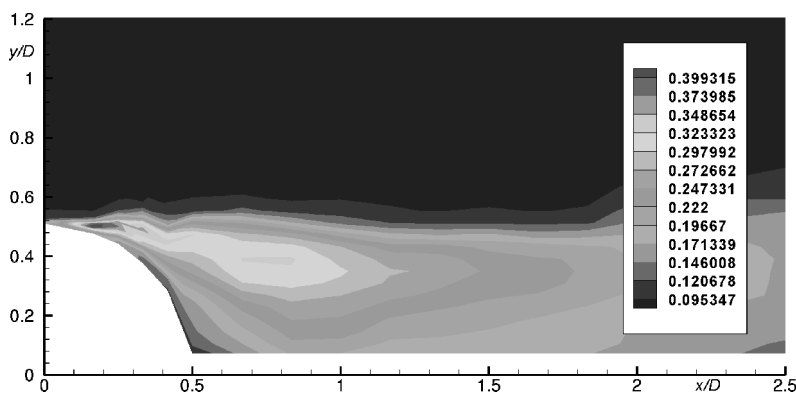

Figure 17. Contours of the measured axial turbulence intensity $(\overline{u^2})^{1/2}/U_0$ behind sphere in a flow with high free-stream turbulence

73

Figures 17 and 18 show the axial and radial turbulent intensity $(\overline{u^2})^{1/2}/U_0$, $(\overline{v^2})^{1/2}/U_0$ and fig. 19 shows Reynolds stress $\overline{uv}/U_0^2$. All turbulence intensities and Reynolds stresses are greater in the case of high free-stream turbulence than in a flow with low turbulence intensity, both with and without trip-wire. Intensification of the mixing process with increasing free-stream turbulence is the main reason for this. A more detailed comparison of the three flows will be presented in the next subsection.
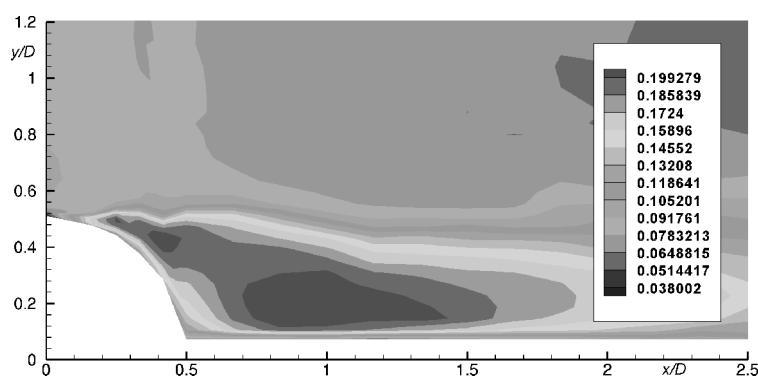

Figure 18. Contours of the measured radial turbulence intensity $(\overline{v^2})^{1/2}/U_0$ behind sphere in a flow with high free-stream turbulence
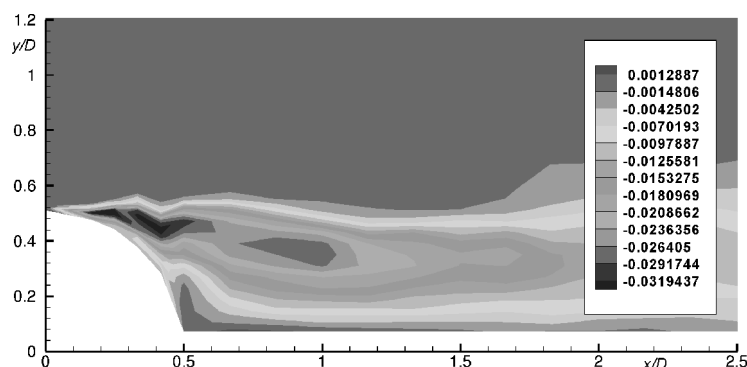

Figure 19. Contours of the measured Reynolds stress $\overline{uv}/U_0^2$ behind sphere in a flow with high free-stream turbulence

Comparison of flows around a sphere

In the previous subsections, contours of the various measured quantities have been shown, with their characteristic levels. In order to enable a direct comparison of the flow features and to asses the effects of the trip-wire and of the high free-stream turbulence, all measured quantities are shown here again using the same plot parameters for the three cases.

74

Figures 20 and 21 show comparison of axial and radial mean velocity components for these three cases. A comparison of contours of axial velocity components, fig.
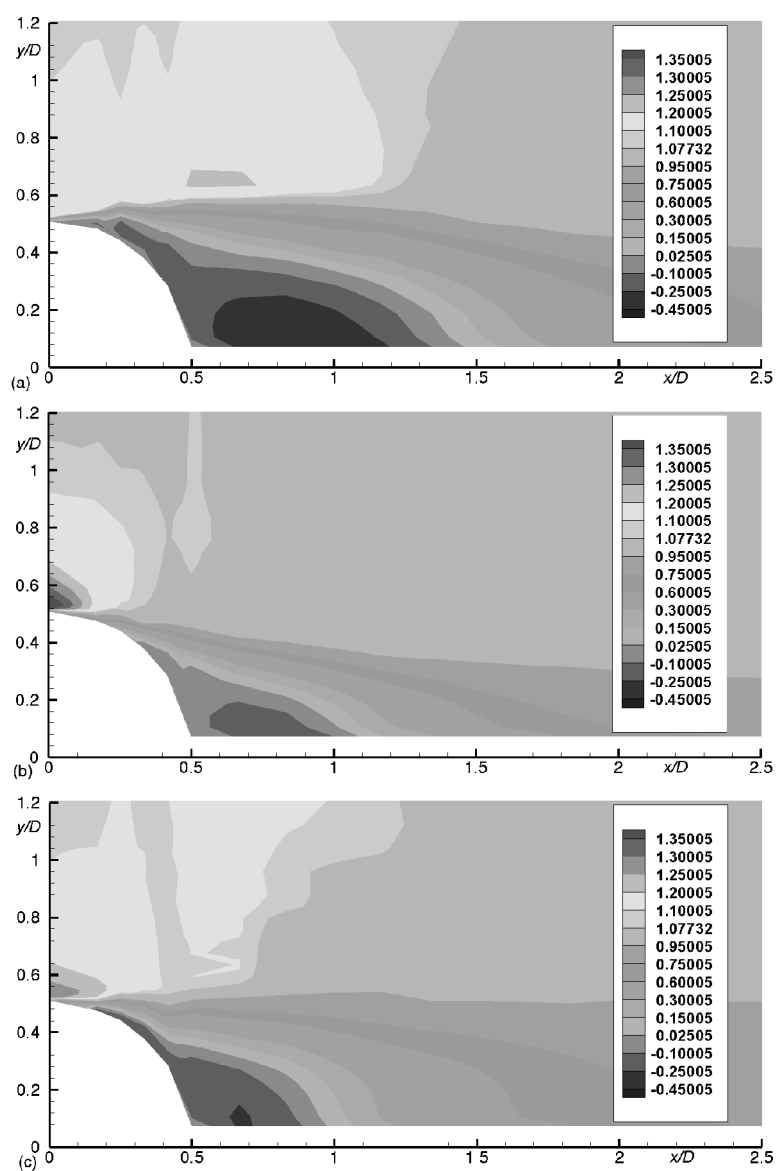

Figure 20. Contours of the measured axial velocity component U/U_0: smooth sphere with low free-stream turbulence (a), sphere with trip-wire and low free-stream turbulence (b), and smooth sphere with high free-stream turbulence (c)

75

20, shows that the highest velocity at the top of the sphere occurs for the case with trip-wire, than for the other cases. Also it is possible to see that later separation increases velocity at the top of the sphere. The length of the recirculation zone is shorter ($L = 1D$) in the case with trip-wire and in a flow with high free-stream turbulence ($L = 1.43D$). Contours of radial velocity in fig. 21 show that in the case with trip-wire negative values of velocity dominate behind the sphere because, due to the transition at the sphere surface (flow moves towards the sting).

　　　　Figures 22, 23, and 24 show that the highest turbulence intensities and Reynolds shear stresses are obtained for the case of a sphere in a flow with high free-stream turbu-
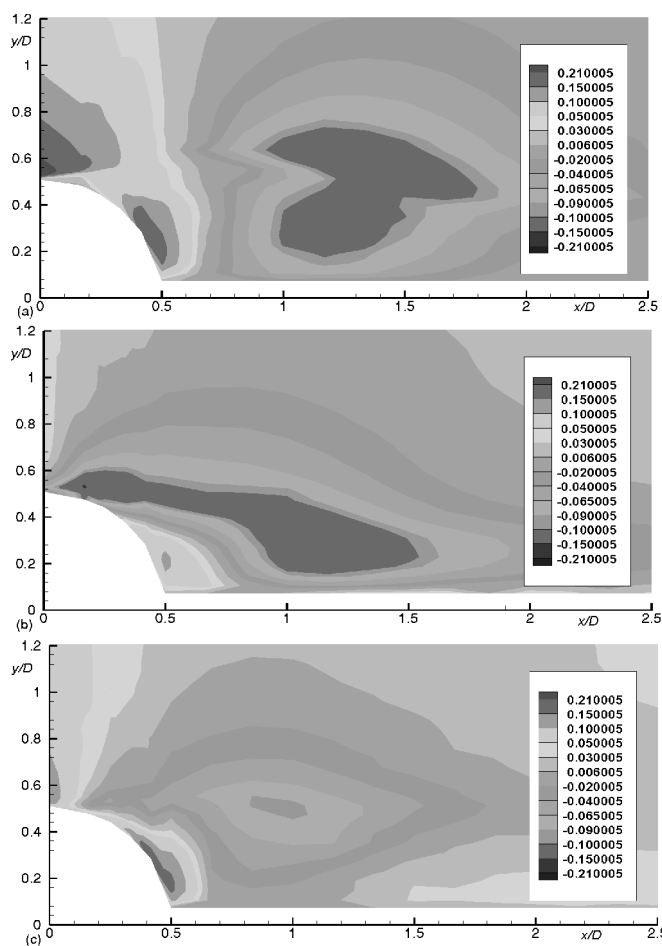

Figure 21. Contours of the measured radial velocity component V/U_0: smooth sphere with low free-stream turbulence (a), sphere with trip-wire and low free-stream turbulence (b), and smooth sphere with
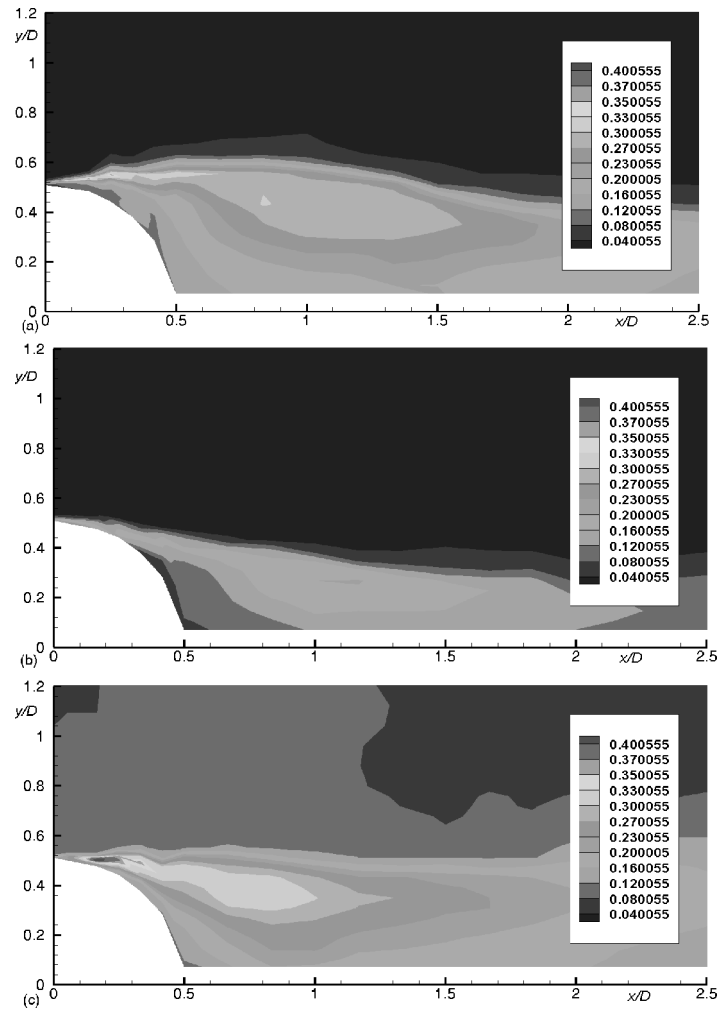
**Figure 22. Contours of the measured axial turbulence inten-
sity $(\overline{u^2})^{\frac{1}{2}}/U_0$: smooth sphere with low free-stream turbulence (a),
sphere with trip-wire and low free-stream turbulence (b), and smooth
sphere with high free-stream turbulence (c)**

lence. Intensification of mixing process between outer flow and shear layer (wake) is the main reason for this. This is one of the reasons why the intensity of the mixing is lower, leading to the lower values of turbulence intensities and Reynolds stresses. On the other hand, increased free-stream turbulence triggers instabilities in the separated shear layer and the wake becomes turbulent earlier than in the case of the smooth sphere with low free-stream turbulence. This can be seen in fig. 22, 23, and 24 for all Reynolds stress

77

components; they attain maximum values shortly after the separation point, and the maximums are higher than for the sphere in a flow with low free-stream turbulence. The wake is narrower in the range $0.5 < x/D < 1.5$ than for the low free-stream turbulence, due to the later separation; however, further downstream ($x/D > 2$), the wake is wider. This again reflects the fact that free-stream turbulence interacts with turbulence generated in the wake, thus intensifying mixing and leading to wake widening, as well as to the higher turbulence levels.
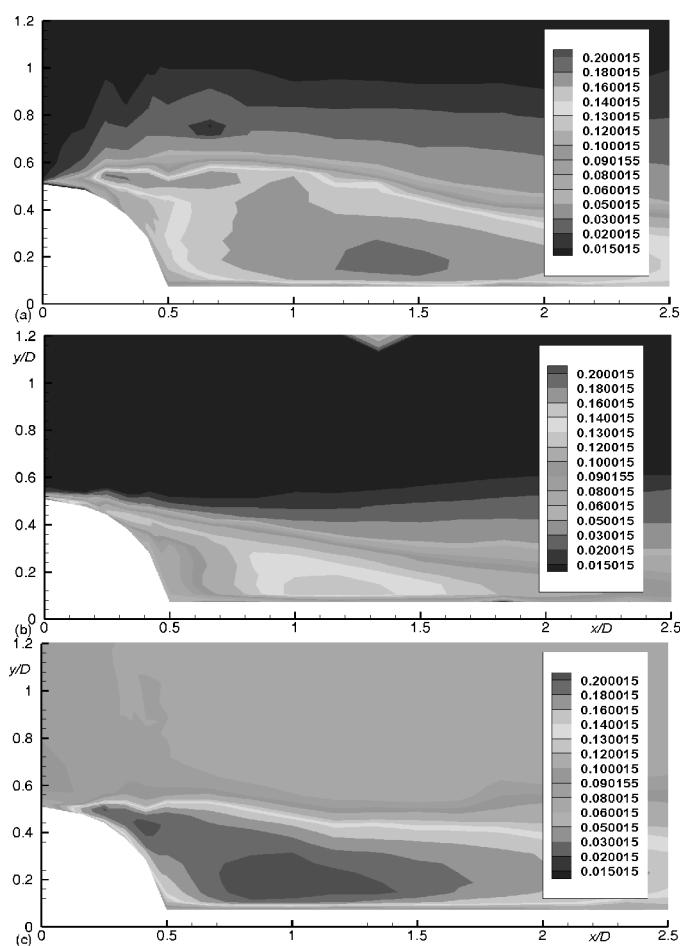

Figure 23. Contours of the measured radial turbulence intensity $(\overline{v^2})^{1/2}/U_0$: **smooth sphere with low free-stream turbulence (a), sphere with trip-wire and low free-stream turbulence (b), and smooth sphere with high free-stream turbulence (c)**

Figure 24. Contours of the measured Reynolds stress $\overline{uv}/U_0^2$: smooth sphere with low free-stream turbulence (a), sphere with trip-wire and low free-stream turbulence (b), and smooth sphere with high free-stream turbulence (c)
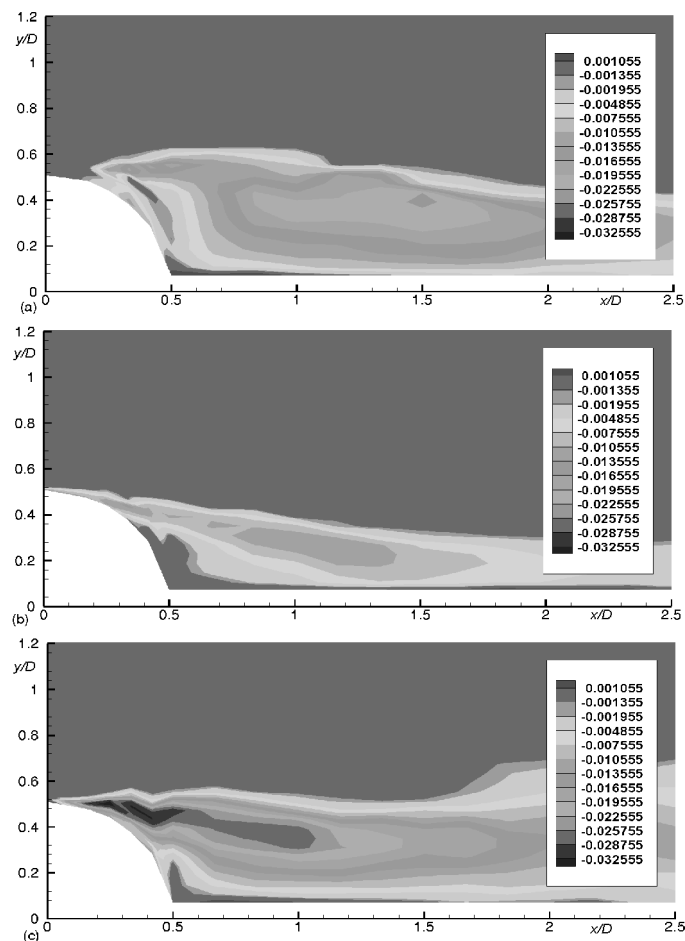
Conclusions

The results of LDA measurements for three different experimental configurations (flow around a smooth sphere, flow around a sphere with trip-wire and flow around a sphere in a flow with high free-stream turbulence) show that flow and turbulence characteristics in the these three cases are substantially different. Experiments were carried out in a wind tunnel at same Reynolds number Re = 51,500, except in the case of a sphere in a flow with high free-stream turbulence where the Reynolds number was Re = = 48,000. Results for the sphere with trip-wire show that the separation point moves

downstream due to the transition of the boundary layer at the sphere surface. Increasing the turbulence intensity in the free-stream also leads to the later separation of the boundary layer. High free-stream turbulence also leads to the increasing of the mixing process and entrainment. This is the reason why the length of the recirculation zone also decreases with increasing free-stream turbulence. The highest turbulence intensity and Reynolds stresses are obtained for the sphere in the flow with the high free-stream turbulence due to a the intensive mixing process. The lowest Reynolds stresses result for the sphere with a trip-wire.

Acknowledgment

Nomenclature

b – bar width, [mm]
D – diameter of sphere, [mm]
d – diameter of sting, [mm]
d_t – diameter of trip wire, [mm]
f – focal length, [mm]
L – length of recirculation zone, [mm]
M – mesh width, [mm]
Re   – Reynolds number, [–]
U_0 – mean velocity, [m/s]
$\overline{U}$ – mean axial velocity, [m/s]
$(\overline{u^2})^{1/2}$ – axial root means square, [m/s]
$\overline{uv}$ – Reynolds shear stress, [m^2/s^2]
$\overline{V}$ – mean radial velocity, [m/s]
$(\overline{v^2})^{1/2}$ – radial root means square, [m/s]
x – axial distance from sphere center, [mm]
y – radial distance from sphere center, [mm]

Greek letters

α_s – angle of separations, [°]

References

[1] Achenbach, E., Experiments on the Flow Past Spheres at Very High Reynolds Numbers, *Journal of Fluid Mechanics, 54* (1972), pp. 565-575

[2]   Bearman, P. W., Turbulence Effects on Bluff Body Mean Flow, *Proceedings,* 3th U. S. National Conference on Wind Engineering, Florida, USA, 1978, pp. LV-1

[3]   Fage, A., The Effects of Turbulence and Surface Rougness on the Drag of a Circular Cylinder, *Reports and Memoranda*, *No. 1283* (1929), pp. 248-255

[4]   Johnson, T. A., Patel, V. C., Flow Past a Sphere up to a Reynolds Number of 300, *Journal of Fluid Mechanics*, *378* (1999), pp. 19-70

[5]   Kim, H. J., Durbin, P. A., Observations of the Frequencies in a Sphere Wake and of Drag Increase by Acoustic Excitation, *Physics of Fluids A, 31* (1988), pp. 3260-3265

[6]   Leder, A., Geropp, D., The Unsteady Flow Structure in the Wake of the Sphere, *Laser Anemometry Advances and Applications*, 1993, pp. 119-125

[7]   Magarvey, R. H., Bishop, L. R., Transition Ranges for Three-Dimensional Wakes, *Canadian Journal of Physics, 39* (1961), pp. 1418-1422

[8]   Raithby, G. D., Eckert, E. R. G., The Effect of Support Position and Turbulence Intensity on the Flow Near the Surface of a Sphere, *Wärme und Stoff, 1* (1968), pp. 87-94

[9]   Sakamoto, H., Haniu, H., A Study of Vortex Shedding from Sphere in a Uniform Flow, *Transactions of the ASME, 112* (1990), pp. 386 – 392

[10] Seidl, V., Development and Use of Parallel Finite Volume Procedure for Flow Simulation Using Unstructured Grid with Local Refinement (in German), Ph. D. thesis, Technical University Hamburg – Harburg, Germany, 1997

[11] Schmid, M., Large Eddy Simulation of Turbulent Flow with Unstructured Grid and with Finite Volume Parallel Methods (in German), Ph. D. thesis, Tehnical University Hamburg – Harburg, Germany, 2001

[12] Taneda, S., Visual Observations of the Flow Past a Sphere at Reynolds Numbers between 10^4 and 10^6, *Journal of Fluid Mechanics*, *85* (1978), pp. 187-192

[13] Wieselberger, C., A Sphere Drag (in German), *Zeitschrift für Mechanik, 5* (1914), pp. 140-144

Author's address:

V. Bakić
VINČA Institute of Nuclear Sciences
Laboratory for Thermal and Energy Research
P. O. Box. 522, 11001 Belgrade
Serbia and Montenegro